GUIDANCE OF A VISION-BASED AUTONOMOUS VEHICLE ON SIDEWALKS FOR USE AS A MACHINE GUIDE DOG[*]

[1]*Yen-Han Chou* (周彦翰) *and* [2]*Wen-Hsiang Tsai* (蔡文祥)

[1]Institute of Computer Science and Engineering
[2]Department of Computer Science
National Chiao Tung University, Hsinchu, Taiwan
Emails: datoyang.cs98g@nctu.edu.tw, whtsai@cis.nctu.edu.tw

ABSTRACT

A vision-based autonomous vehicle system with a tilted 2-mirror omni-camera for use as a machine guide dog in outdoor sidewalk environments is proposed. The vehicle is guided by localization of along-path landmarks, including curb lines, hydrants, and light poles. In environment learning, a navigation map including a navigation path, along-path landmark locations, and relevant environment processing parameters is constructed. In the navigation process, a new vertical space line detection technique for localizing light poles and hydrants appearing in omni-images is proposed. Also proposed are a new dynamic obstacle detection technique which uses ground matching tables to localize obstacles, as well as dynamic techniques for exposure and threshold adjustments for adapting the system to varying outdoor conditions. Good experimental results show the feasibility of the proposed system.

Keywords: *autonomous vehicle navigation, landmark detection, vehicle localization, learning, guidance.*

1. INTRODUCTION

Guide dogs provide special services to blind people. According to the information provided by Taiwan Foundation for the Blind and Taiwan Guide Dog Association, there are more than fifty thousand blind people but just thirty trained guide dogs in Taiwan. Hence, it is desired in this study to design a vision-based autonomous vehicle with wide-view computer vision and an along-path localization capability for use as a machine dog on the sidewalk.

About the visual device for use on an autonomous vehicle, in contrast with a traditional projective camera, an omni-directional camera (omni-camera) has the advantage of having a larger field of view (FOV), and so is more suitable for the purpose of monitoring a larger environment area. In this study, we use a specially-designed omni-camera with two mirrors as the visual device on an autonomous vehicle.

One way to localize a vehicle is to use landmarks. Yu and Kim [1] detected particular landmarks in home environments and localized the vehicle by the distance between the vehicle and each landmark. Tasaki et al. [2] conducted vehicle self-localization by tracking space points with scale- and rotation-invariant features. Wu and Tsai [3] detected circular landmarks on ceilings to accomplish indoor vehicle navigation. Siemiątkowska and Chojecki [4] used the wall plane landmarks to localize a vehicle. Courbon et al. [5] conducted vehicle localization by memorizing key views in order along a path and compared the current image with them in navigation. Besides self-localization, the autonomous vehicle has to own more capabilities when navigating in more complicated environments. Obstacle avoidance is an essential ability for vehicle navigation, and a mobile robot system with this capability was proposed by Kumar [6]. The mobile robot proposed by Mühlbauer et al. [7] not only can navigate by sidewalk following in the urban area, but also can interact with people.

The goal of this study is to train and then guide automatically an autonomous vehicle equipped with a two-mirror omni-camera mentioned above to work as a guide dog to navigate on a sidewalk with colored curb lines. The system process includes two phases: learning and navigation. In the learning process, we guide the autonomous vehicle to navigate on a sidewalk and "memorize" along-path landmarks, including light poles and hydrants, as well as some related environment parameters. Then, in the navigation process the system follows the curb line on one side of the sidewalk and localizes itself node by node using the learned along-path landmarks to navigate forward to an appointed goal. Some other strategies for reliable navigation such as obstacle avoidance and dynamic parameter adjustment are also proposed for this system. Contributions made in this study include at least the following.

(1) A method of training an autonomous vehicle for outdoor navigation on sidewalks using commonly-seen landmarks and a navigation map is proposed.

(2) A new space line detection technique using the space-mapping approach [8] is proposed.
(3) New techniques for detecting hydrants and light poles for vehicle localization are proposed.
(4) A technique of following sidewalk curb lines for vehicle navigation is proposed.
(5) A new obstacle avoidance technique based on the use of a ground matching table is proposed.
(6) Dynamic camera exposure and image threshold adjustment techniques for stable vehicle guidance in sidewalk environments are proposed.

The details of the proposed autonomous vehicle system will be introduced in the following sections, with the learning process described in Section 2, the navigation strategy in Section 3, the proposed hydrant and light pole detection techniques using a new space line detection technique in Section 4, the proposed curb line following and obstacle avoidance techniques in Section 5, and some experimental results in Section 6, followed by conclusions in the last section.

2. LEARNING PROCESS

In the learning process, the camera system is calibrated first. Then, the vehicle is navigated through a sidewalk to visit desired spots and landmarks to construct a *navigation path* consisting of *nodes*. Related guidance parameters are also computed. A *navigation map* for use in the navigation process is established finally.

2.1 Construction of Pano-mapping Tables

The entire system configurations and the used two-mirror omni-camera are shown in Fig. 1. The camera system consists of a bigger hyperboloidal-shaped mirror and a smaller one, called *Mirror A* and *Mirror B*, respectively, subsequently in this paper. This camera system is slanted up for an angle of γ and then placed on the vehicle for the purpose of "seeing" more of the scene in front of the vehicle system.
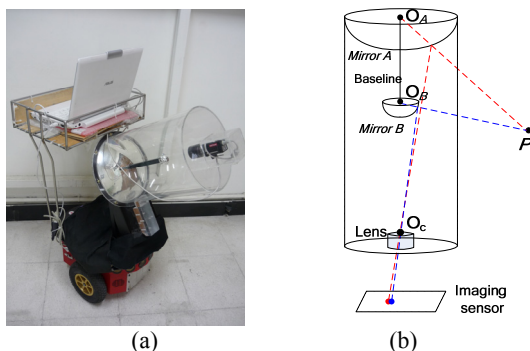
Fig. 1: System configurations. (a) The vehicle. (b) Illustration of used camera system.

Instead of computing the camera's intrinsic and extrinsic parameters, we adopt a space-mapping technique [8] to "calibrate" the camera system used in this study. The idea is to establish a so-called *pano-mapping table* to record the relations between image points and corresponding world-space points. More

specifically, as illustrated in Fig. 2, a light ray going through a world-space point P with an elevation angle α and an azimuth angle θ is projected onto an image point p with coordinates (u, v) in the omni-image. A pano-mapping table as illustrated by Table 1 specifies the mapping relations between the coordinates (u, v) of each image point p and the azimuth-elevation angle pair (θ, α) of the corresponding world-space point P. The table is established once in advance and can be used forever by table lookup to get the corresponding 3D data, (θ, α), for each given image pixel with coordinates (u, v), and vice versa. For this study, we construct two of such tables for Mirrors A and B, respectively.
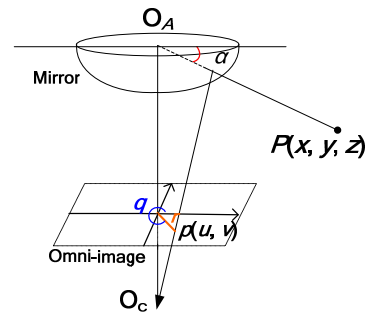
Fig. 2: Principle of imaging a point P using an omni-camera.

Table 1: A pano-mapping table with size $M \times N$.

	θ_1	θ_2	θ_3	θ_4	…	θ_M
α_1	(u_{11}, v_{11})	(u_{21}, v_{21})	(u_{31}, v_{31})	(u_{41}, v_{41})	…	(u_{M1}, v_{M1})
α_2	(u_{12}, v_{12})	(u_{22}, v_{22})	(u_{32}, v_{32})	(u_{42}, v_{42})	…	(u_{M2}, v_{M2})
α_3	(u_{13}, v_{13})	(u_{23}, v_{23})	(u_{33}, v_{33})	(u_{43}, v_{43})	…	(u_{M3}, v_{M3})
α_4	(u_{14}, v_{14})	(u_{24}, v_{24})	(u_{34}, v_{34})	(u_{44}, v_{44})	…	(u_{M4}, v_{M4})
...	…	…	…	…	…	…
α_N	(u_{1N}, v_{1N})	(u_{2N}, v_{2N})	(u_{3N}, v_{3N})	(u_{4N}, v_{4N})	…	(u_{MN}, v_{MN})

2.2 Learning of Landmarks

For the purpose to localize the vehicle during the navigation process, we use the landmarks of curb lines, light poles, and hydrants in this study, which are commonly-seen objects on sidewalks. Furthermore, to deal with different outdoor environments, two sets of parameters are recorded for each landmark detection task. One is used to specify an *environment window* which is a rectangular region pre-defined to describe the landmark position in the omni-image. The other is used to specify an *environment intensity* which is the mean image intensity value in the environment window of an omni-image acquired by the camera system after manually adjusting the camera exposure to yield a suitable image illumination which leads to successful landmark detection. By using this environment intensity as a reference, the desired landmark can be well detected afterward in the vehicle navigation process.

3. NAVIGATION STRATEGY

3.1 Principle of Navigation Process

The vehicle is guided to visit sequentially each node recorded in the navigation map by following the curb

line and avoiding collisions with along-path known or unknown obstacles. Also, the vehicle localizes its position by landmarks, corrects the odometer readings and adjusts relevant guidance parameters using techniques of dynamic image threshold and camera exposure adjustment at each path node.

3.2 Vehicle Localization by Curbs and Landmarks

The odometer readings provide posture information of the vehicle, including its position (P_x, P_y) and orientation P_{th} in the world space when navigating to each path node. These data become imprecise owing to incremental mechanic errors after the vehicle navigates for a certain time period. Thus, it is desired to adjust the vehicle posture node by node in the navigation. We use the recorded curb line orientations as well as hydrant or light pole positions to localize the vehicle in this study.

In more detail, as shown in Fig. 3, in each navigation cycle, after adjusting the vehicle to orient to the recorded direction P_{th} at a certain node, we detect the nearby curb line segment to obtain its slope angle θ' with respect to the vehicle. Then, we retrieve the recorded slope angle θ of the curb line segment at the current node, compute the difference $\theta_{adj} = \theta' - \theta$, modify the orientation reading of the vehicle's odometer for the amount of θ_{adj}, and take the result to be the correct current orientation P_{th}' of the vehicle.

Next, we detect the hydrant or light pole landmark at the current node, if any, to obtain its location (X_{lm}, Y_{lm}) with respect to the vehicle. Then, we retrieve the recorded position (P_X, P_Y) of the hydrant or light pole, and use them together with the correct vehicle orientation P_{th}' to compute the correct vehicle position (X_c, Y_c) in the world space by:

$$\begin{bmatrix} X_c \\ Y_c \end{bmatrix} = \begin{bmatrix} P_X \\ P_Y \end{bmatrix} + \begin{bmatrix} \cos P_{th}' & \sin P_{th}' \\ -\sin P_{th}' & \cos P_{th}' \end{bmatrix} \begin{bmatrix} X_{lm} \\ Y_{lm} \end{bmatrix}.$$

Finally, we replace imprecise position readings of the odometer, (P_X', P_Y'), by the computed position (X_c, Y_c).

3.3 Dynamic Exposure Adjustment

According to the experimental result shown in Fig. 4, we found that there exits a specific range of camera exposure values in which the exposure value has an approximate linear relation with the image intensity Y. Thus, we can estimate an appropriate value E for camera exposure adjustment before image taking by:

$$E = f_{exp}(Y) = mY + b. \tag{1}$$

Thus, in this study we propose an efficient 2-stage scheme to automatically adjust the camera exposure value to obtain the previously-mentioned environment intensity Y in the previously-mentioned environment window in an image. First, we use a bisection scheme to adjust the exposure to find a specific range $[E_1, E_2]$ with which yields a range $[Y_1, Y_2]$ of proper image intensities. Next, we utilize linear interpolation to adjust the exposure to a value E_d which yields the desired environment intensity Y by the following equation:

$$E_d = \frac{Y - Y_1}{Y_2 - Y_1} \times (E_2 - E_1) + E_1. \tag{2}$$
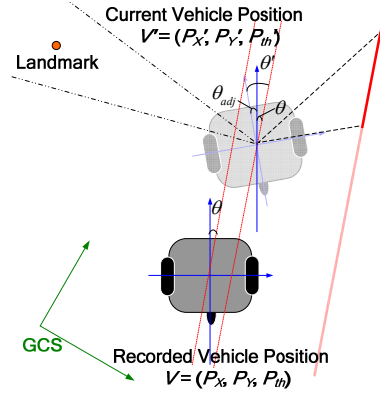
Fig. 3: A recoded vehicle position V and the current vehicle position V'.
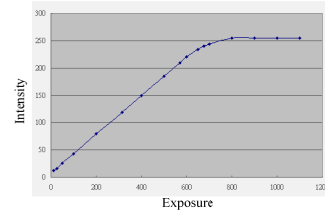
Fig. 4: A relationship between the exposure value and the image intensity obtained in an experiment.

4. LIGHT POLE AND HYDRANT DETECTION USING NEW SPACE LINE DETECTION TECHNIQUE

In contrast to the function of a traditional projective camera, the projection of a space line on an omni-image using an omni-camera is not a line, but a conic-section curve [9]. Wu and Tsai [9] detected such curves formed by an H-shaped landmark for use in automatic helicopter landing using the hyperboloidal mirror parameters and some geometric relationship.

Based on the use of pano-mapping tables which involve no camera parameters and so are more convenient for applications, we propose a new space line detection technique in this study. Instead of deriving the formula of the projected conic section curve of a space line in the omni-image, we obtain a formula which describes a space plane going through the space line and the mirror center. Furthermore, for the simpler type of space line which is *perpendicular* to the ground, we can derive an analytic formula to compute its 3D position information directly based on the results of the proposed line detection method. Finally, by the use of this vertical space line detection technique, we also propose new schemes for light pole and hydrant localization in this study. The details are described in the following.

4.1 Proposed Technique for Space Line Detection

Suppose that a space line L is projected by Mirror A onto an omni-image as shown in Fig. 5 and that P is an

arbitrary space point on *L*. Firstly, we consider a way to represent the vector V_P which goes through *P* and the mirror center O_A in the camera system. As shown in Fig. 6(a), the light ray which goes through the space point *P* is reflected by Mirror *A* to project onto the image plane to form an image point *p* with coordinates (*u*, *v*). By looking up the pano-mapping table using (*u*, *v*), we can get the elevation-azimuth angle pair (α, θ) of *P*. Accordingly, it can be figured out from Fig. 6(a) that vector V_P can be described as $(P_x', P_y', P_z')^T$ with $P_x' = \cos\alpha \times \cos\theta$, $P_y' = \cos\alpha \times \sin\theta$, $P_z' = \sin\alpha$ where *T* means transpose. But the omni-camera is tilted for an angle of γ as mentioned previously. Therefore, the vector should be rotated for γ for use in an un-tilted camera coordinate system (CCS) as shown in Fig. 6(b), leading to the following result:

$$V_P = \begin{bmatrix} P_x \\ P_y \\ P_z \end{bmatrix} = \begin{bmatrix} 1 & 0 & 0 \\ 0 & \cos(-\gamma) & -\sin(-\gamma) \\ 0 & \sin(-\gamma) & \cos(-\gamma) \end{bmatrix} \begin{bmatrix} P_x' \\ P_y' \\ P_z' \end{bmatrix}$$
$$= \begin{bmatrix} \cos\alpha \times \cos\theta \\ \cos\alpha \times \sin\theta \times \cos\gamma + \sin\alpha \times \sin\gamma \\ -\cos\alpha \times \sin\theta + \sin\alpha \times \cos\gamma \end{bmatrix}. \quad (3)$$
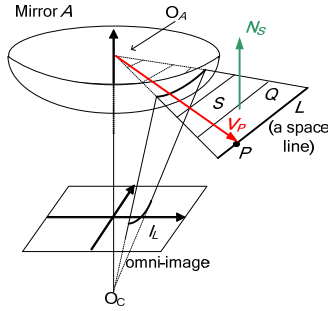
Fig. 5: A space line *L* projected onto omni-image as a curve I_L.

(a)   (b)
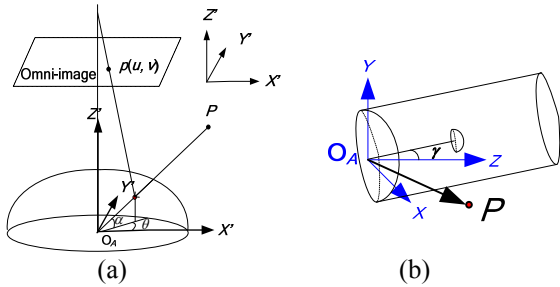
Fig. 6: Illustrations of vector V_P from O_A to *P*. (a) A space point with elevation angle α and azimuth angle θ. (b) Camera coordinate system (CCS).

Next, considering the space line *L* projected onto the omni-image as the image line I_L as shown in Fig. 5, we want to find a space plane *S* which goes through *L* and the mirror center O_A. For this, suppose that the normal vector of *S* is denoted as $N_S = (l, m, n)$ and let *Q* be a point on *S* with coordinates (*X*, *Y*, *Z*). Since N_S is perpendicular to the vector V_Q which goes through *Q* and the mirror center O_A with coordinates (0, 0, 0), we can derive the following equation to describe (*X*, *Y*, *Z*):

$$N_S \cdot V_Q = (l, m, n) \cdot (X, Y, Z) = lX + mY + nZ = 0. \quad (4)$$

where "$\cdot$" means the inner product operation. Similarly, vector V_P is also perpendicular to N_S, so we have:

$$N_S \cdot V_P = (l, m, n) \cdot (P_x, P_y, P_z) = lP_x + mP_y + nP_z = 0. \quad (5)$$

By Eq. (3), we can transform Eq. (5) to be:

$$l + m \times \frac{\cos\alpha \times \sin\theta \times \cos\gamma + \sin\alpha \times \sin\gamma}{\cos\alpha \times \cos\theta}$$
$$+ n \times \frac{-\cos\alpha \times \sin\theta + \sin\alpha \times \cos\gamma}{\cos\alpha \times \cos\theta} = 0. \quad (6)$$

It is desired to obtain from Eq. (6) the three unknown parameters *l*, *m*, and *n* which represent the normal of the space plane *Q*. For this purpose, we divide Eq. (6) by *n* to get the following form:

$$B + Aa_0 + a_1 = 0 \quad (7)$$

where $A = m/n$, $B = l/n$, and

$$a_0 = \frac{\cos\alpha \times \sin\theta \times \cos\gamma + \sin\alpha \times \sin\gamma}{\cos\alpha \times \cos\theta},$$
$$a_1 = \frac{-\cos\alpha \times \sin\theta + \sin\alpha \times \cos\gamma}{\cos\alpha \times \cos\theta}.$$

Eq. (7) means that we may use two parameters *A* and *B* to represent the original three ones *l*, *m*, *n*. Accordingly, we can use a simple 2D Hough transform technique to obtain the parameters *A* and *B*.

Furthermore, if *L* is a *vertical* space line (perpendicular to the ground in the world space), it means that the normal vector of the space plane *S* is parallel to the ground. Then, it is easy to figure out that *m* is equal to zero and Eq. (7) can be reduced to be of the form:

$$B = -a_1 \quad (8)$$

where $B = l/n$ and

$$a_1 = \frac{-\cos\alpha \times \sin\theta + \sin\alpha \times \cos\gamma}{\cos\alpha \times \cos\theta}.$$

Accordingly, we can use an even simpler 1D Hough transform to find the parameter *B*. The detail of this transform is described in the following.

First, establish a 1D Hough space *H* with parameter *B* and initialize all cell counts to be zero. Also, for each point *p* on the vertical line *L* at coordinates (*u*, *v*) in the given omni-image, look up the pano-mapping table to obtain an elevation and azimuth angle pair (α, θ), compute *B* by Eq. (8) using θ and α, and increment by 1 the value of the cell with parameter *B* in *H*. Finally, find the cell value with the maximum value B_o in the Hough space *H* as the desired parameter *B* appearing in Eq. (8), which describes the vertical line *L*.

4.2 3D Data Computation for a Vertical Space Line

A vertical space line *L* is projected by Mirrors *A* and *B* onto the image plane as two image lines I_{L1} and I_{L2}, respectively, as shown in Fig. 7. The center O_A of Mirror *A* is located at coordinates (0, 0, 0) in the camera

coordinate system (CCS). Thus, denoting the length of the *baseline* connecting the two mirror centers O_A and O_B as b and taking into consideration of the tilt angle γ of the camera system, we can derive easily the position of the center O_B of Mirror B to be $(0, b\sin\gamma, b\cos\gamma)$ in the CCS. Next, according to Eq. (4), the equations of the two space planes S_1 and S_2 going through L and the mirror centers, O_A and O_B, respectively, can be described by:

$$l_1X + m_1Y + n_1Z = 0; \tag{9}$$
$$l_2X + m_2(Y - b\sin\gamma) + n_2(Z - b\cos\gamma) = 0 \tag{10}$$

where (l_1, m_1, n_1) represents the normal vector of S_1 and (l_2, m_2, n_2) represents that of S_2.
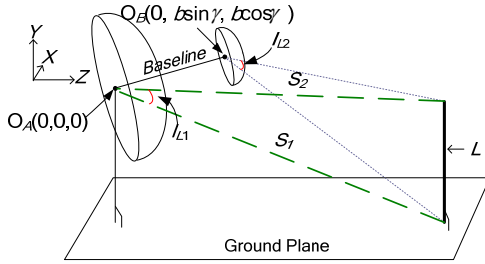
Fig. 7: A vertical space line projected onto two mirrors in the used two-mirror omni-camera.

In addition, by the reason that the space line L is perpendicular to the ground, we know that m_1 and m_2 are both zero. Thus, the above two space plane equations may be reduced to be:

$$l_1X + n_1Z = 0; \tag{11}$$
$$l_2X + n_2(Z - b\cos\gamma) = 0 \tag{12}$$

or equivalently, to be:

$$B_1X + Z = 0; \tag{13}$$
$$B_2X + (Z - b\cos\gamma) = 0 \tag{14}$$

where $B_1 = l_1/n_1$ and $B_1 = l_2/n_2$. Solving Eqs. (13) and (14), we can obtain the following equations to describe the position of the vertical space line L:

$$X = \frac{b\cos\gamma}{B_2 - B_1} ; \quad Z = \frac{-B_1 b\cos\gamma}{B_2 - B_1} \tag{15}$$

where $B_1 = l_1/n_1$, $B_1 = l_2/n_2$.

4.3 Light Pole Localization for Vehicle Guidance

The idea of the proposed method for light pole localization is to use the two vertical boundary lines of the light pole to estimate the position of the light pole using the formulas derived in the last section.

Firstly, we apply Canny edge detection to the omni-image to obtain an edge point image which includes the boundary points of the light pole. Then, we apply the above-mentioned 1D Hough transform to find the parameters B_1 and B_2 of Eq. (8) which describe the two vertical boundary lines of the light pole, respectively. Accordingly, we compute the locations of the two light pole boundary lines on the ground, denoted as G_{in} and

G_{out}, respectively, in the CCS using Eq. (15). Finally, we compute the distance d between G_{in} and G_{out}, and check if d is close to the pre-measured diameter of the light pole within a tolerable range — if so, then we compute the center position between G_{in} and G_{out} for use as the light pole position; otherwise, regard the detected object as not a light pole. A result of light pole detection and localization using the above method is shown in Fig. 8.
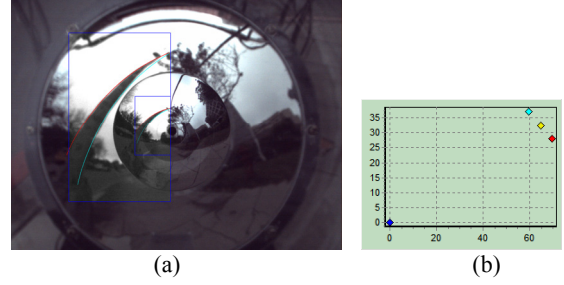
Fig. 8: A result of light pole detection. (a) Detected boundary lines (one in red and the other in green). (b) Localized light pole (yellow dot) between two boundary lines (red and light blue dots) with respect to vehicle (blue dot).

4.4 Hydrant Localization for Vehicle Guidance

To detect a hydrant in an omni-image, we utilize the hue and saturation values in the HSI color model to extract the hydrant contour in order to ignore the influence of the varying image intensity caused by the time-changing lighting condition in the outdoor environment. Specifically, after applying the dynamic exposure adjustment process mentioned previously, we scan each pixel p in the input image I and compute its hue value h_{uv} and saturation value s_{uv}, and if h_{uv} is within a certain range R_H of hue values and s_{uv} is within another range R_S of saturation values, then we regard p as a hydrant feature point. Examples of hydrant feature point detection results are shown in Fig. 10(a) and 10(b).

After all of the feature points are extracted, we apply the erosion and dilation operations to them to remove small noise points, and conduct connected component labeling to find the largest connected component M in input image I. Then, we compute the covariance matrix C_x of the image coordinates of all the feature points of M using principal component analysis to obtain two eigenvalues λ_1 and λ_2, and two corresponding eigenvectors $e_1(u_1, v_1)$ and $e_2(u_2, v_2)$ of C_x. Finally, we compute the length ratio η of the two eigenvalues of C_x and the rotational angle ω between the ICS for use as the *features* of the hydrant, as illustrated in Fig. 9, according to the following equations: $\omega = \tan^{-1}(v_1/u_1)$, $\eta = \lambda_1/\lambda_2$.

Moreover, because different projections of the same hydrant on omni-images taken at different positions are usually similar, we can record as many different extracted hydrant contours as possible in order to "learn" the hydrant contour more precisely. For this, we guide the vehicle to take a number of omni-images from different directions at different positions. And for

each obtained image I_i, we compute two features ω_i and η_i in the previous way after extracting the hydrant feature points. Then, from all the values of ω_i and η_i, we select their maximum and minimum ones to form two ranges of the hydrant features. After this learning process, if the computed rotational angle ω and the length ratio η in hydrant detection are not in the learned ranges, we decide that the result of detection is not a hydrant, and vice versa.

(a)   (b)
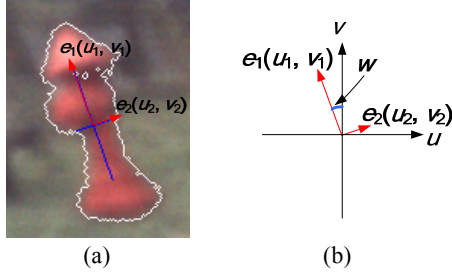
Fig. 9: Principal component analysis for hydrant detection. (a) Detected principal axis and eigenvectors. (b) Illustration of rotational angle ω.

The idea of the proposed hydrant localization method is to detect the vertical axis line of the hydrant using principal component analysis, and localize the hydrant by this line. More specifically, we compute the center C_A with coordinates (u_A, u_A) of the hydrant using its feature points detected in a pre-selected image region formed by light rays reflected by Mirror A. We also compute similarly the center C_B with coordinates (u_B, u_B) of the hydrant using its feature points detected in a pre-selected image region formed by light rays reflected by Mirror B. Both the image points C_A and C_B correspond to the center point of the hydrant in the real-world space. Then, by using (u_A, v_A) and (u_B, v_B), we look up the pano-mapping table to obtain the corresponding elevation-azimuth angle pairs (α_A, θ_A) and (α_B, θ_B) of C_A and C_B, respectively. And by Eq. (8), we compute the parameter B_A corresponding to C_A using (α_A, θ_A) as well as the parameter B_B corresponding to C_B using (α_B, θ_B). Finally, by the use of B_A and B_B, we can find out the axis L of the hydrant through C_A and C_B in the input image, and by Eq. (15) we can compute the position of L for use as that of the hydrant. A result of hydrant detection and localization using the above method is shown in Figs. 10(c) and 10(d).

5. LINE FOLLOWING AND OBSTACLE AVOIDANCE TECHNIQUES

5.1 Curb Line Detection and Following Technique

When not using landmarks to estimate its location, the vehicle system navigates on the sidewalk mainly by curb line following, which includes three major stages as described in the following.

Stage 1 — extracting and locating curb feature points.

First, we detect the curb feature points in the image region formed by light rays reflected by Mirror A using the HSI color model by the method we use for detecting the hydrant as discussed previously. Then, we conduct the erosion and dilation processes to eliminate small noise points. Also, we scan each feature point in a raster-scan order to find the inner boundary points of the curb line. And by looking up the pano-mapping table, we get the elevation-azimuth angle pair (α, θ) using the image coordinates (u, v) of each boundary point P so found. Assume that the coordinates of P in the CCS are (X, Y, Z) which we want to compute now. Then, the vector V_P from P to Mirror A's center O_A in the CCS may be described by Eq. (3), which we repeat below:

$$V_P = \begin{bmatrix} P_x \\ P_y \\ P_z \end{bmatrix} = \begin{bmatrix} \cos\alpha \times \cos\theta \\ \cos\alpha \times \sin\theta \times \cos\gamma + \sin\alpha \times \sin\gamma \\ -\cos\alpha \times \sin\theta + \sin\alpha \times \cos\gamma \end{bmatrix}.$$

(a)   (b)

(c)   (d)
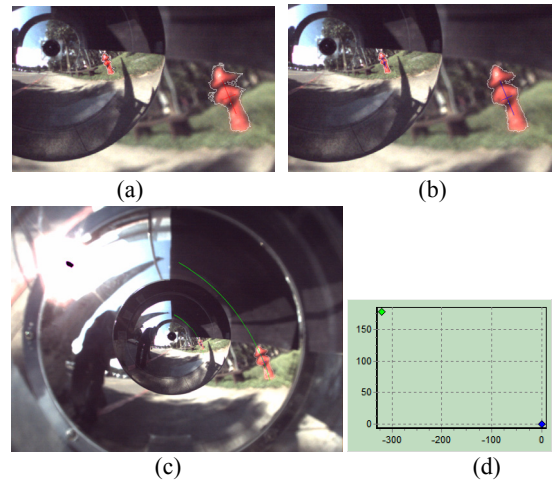
Fig.10: Results of hydrant detection and localization. (a) Segmentation result using original threshold values. (b) Segmentation result after dynamic exposure adjustment and thresholding. (c) Detected vertical axis of hydrant (green lines). (d) Estimated hydrant position (green dot).

Besides, because the height H of the center of *Mirror A* is known in advance, we can derive further that $Y = -H$. Hence, by the proportions among P_x, P_Y, and P_Z and the known value of Y, the coordinates X and Z may be computed to be:

$$X = \frac{-H \times (\cos\alpha \times \cos\theta)}{\cos\alpha \times \sin\theta \times \cos\gamma + \sin\alpha \times \sin\gamma};$$

$$Z = \frac{-H \times (-\cos\alpha \times \sin\theta + \sin\alpha \times \cos\gamma)}{\cos\alpha \times \sin\theta \times \cos\gamma + \sin\alpha \times \sin\gamma}. \quad (16)$$

Stage 2 — curb line localization.

Using the computed positions (X, Y, Z) of the boundary points of the curb line, we adopt a line regression scheme to compute the equation of the line on the *X-Z* plane with the following equation:

$$Z = aX + b. \quad (17)$$

Next, we compute the sum of the square errors S_e of fitting the boundary points to a line by the following equation:

$$S_e = \sum_{i=1}^{n} [Z_i - (aX_i + b)]^2. \qquad (18)$$

Accordingly, we apply the proposed dynamic threshold adjustment scheme to adjust the saturation threshold values in a pre-learned range to detect the curb line and find the fitting line L_{best} with the minimum sum of square errors. Then, by Eq. (17), we compute the slope angle θ of L_{best} with respect to the moving direction of the vehicle and the distance d of L_{best} to the vehicle by the following equation:

$$\theta = \tan^{-1}(1/a); \quad d = |b|/\sqrt{1+a^2} . \qquad (19)$$

Stage 3 — navigation by line following

According to the computed θ and d above, we adjust the speed and orientation of the vehicle to keep the navigation path at an appreciate distance to the curb line and parallel to the curb line if the vehicle is at a position with a safe distance to the curb. Otherwise, we slow down the vehicle and turn it progressively to make it to be toward a safe region with respect to the curb line in order to prevent it from falling out of the sidewalk. A result of curb line detection is shown in Fig. 11.
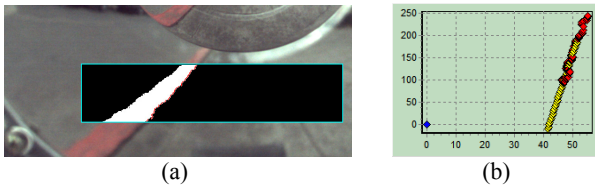
Fig.11: Curb line detection. (a) Segmentation result. (b) Extracted curb points (red dots) and fitting line (yellow dots).

5.2 Obstacle avoidance technique

A ground point will be projected by the two mirrors onto the image plane at two different positions. Accordingly, the idea of the proposed obstacle detection technique is to record first the relation between every two manually-selected *corresponding* ground points in the image regions R_A and R_B formed respectively by light rays reflected by Mirrors A and B, respectively, into a specific table, called *ground matching table* T_m, as illustrated in Fig. 12, and then to use T_m to inspect an object to see whether it is flat on the ground or not for the purpose of detecting obstacles on the navigation path. More details of the proposed method for the learning and navigation phases are described next.

The learning stage ---

In the learning stage, after setting the ground matching table T_m, if the two corresponding image points listed in T_m, which appear in R_A and R_B, respectively, are both projections from a single *ground* point as shown in Fig. 13(a), then their intensity values must be identical or very close in magnitude. However, if there is an obstacle appearing in R_A or R_B as shown in Fig. 12(b), then the two corresponding image points in R_A and R_B will not both be projections of a single ground point G, but be a projection of G and another of an object point F so that their intensity values will be different. Based on observation of this phenomenon, we

can detect obstacle object points in the following way: look up the ground matching table T_m to get every pair of corresponding image points and check their intensity values: if different, then label the image points as coming from an obstacle object point; else, from a ground point. After collecting the obstacle object points found in this way, we compute finally the mean H_{obs} and the variance Var_{obs} of the hue values of each point in the HSI color model for use in the navigation phase.
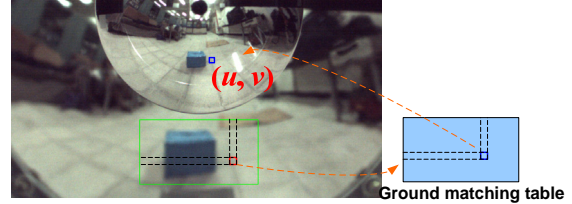
Fig. 12: Illustration of constructing the ground matching table.
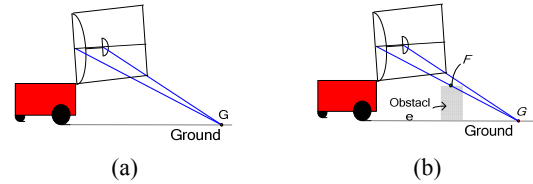
Fig. 13: Two side views of the vehicle and a ground P. (a) Without obstacles. (b) With an obstacle in front.

The navigation phase ---

In the navigation phase, by the use of the HSI color model, we classify the image points by the learned color information, H_{obs} and Var_{obs}, of the obstacle into obstacle points if the hue value of a point is within the distance of two Var_{obs} from H_{obs}. Then, we detect the obstacle bottom boundary by scanning each radial line in the image, starting from the lower image boundary; and takes the first found feature points as the bottom boundary points. A result of such obstacle bottom boundary detection is shown in Fig. 14. Furthermore, for each detected obstacle bottom boundary point, we look up the pano-mapping table to find corresponding elevation and azimuth pair (α, θ), and use Eq. (16) to compute the position of the point. Finally, we calculate the average of the positions of all the bottom boundary points for use as the obstacle location. Finally, to conduct obstacle avoidance, the approach we use is to insert additional nodes into the navigation path to guide the vehicle to change its path to pass the obstacle, as illustrated in Fig. 15.

6. EXPERIMENTAL RESULTS

Many learning and navigation processes have been conducted successfully in our experiments After the learning process, a navigation map is constructed. An example of such maps is shown in Fig. 16. In the navigation process, the vehicle navigated alone the recorded navigation path nodes by curb line following. By the techniques of the dynamic exposure and threshold adjustment, the vehicle detected pre-selected landmarks in images acquires with suitable camera

exposures and localized their positions with respect to the vehicle. Also, after detecting an obstacle, the vehicle created a new path with extra nodes to pass the obstacle without collisions. The process is repeated until the vehicle reached a terminal node. A path map with a record of the visited nodes in a navigation process is shown in Fig. 17.

(a)   (b)
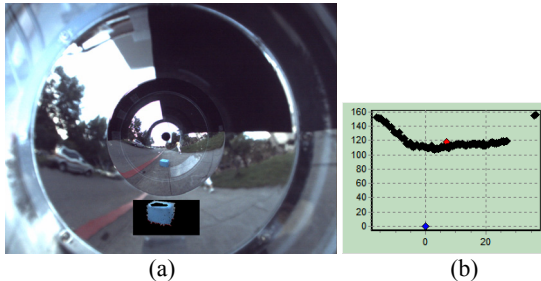
Fig.14: Results of dynamic obstacle detection and localization. (a) Segmentation result with obstacle bottom detected (red points). (b) Estimated obstacle position (red point) as average of detected obstacle bottom points.
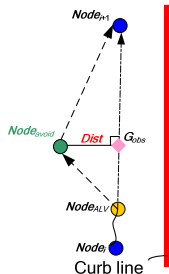
Fig. 15: Illustration of inserting a path node $Node_{avoid}$ for obstacle avoidance in original navigation path.
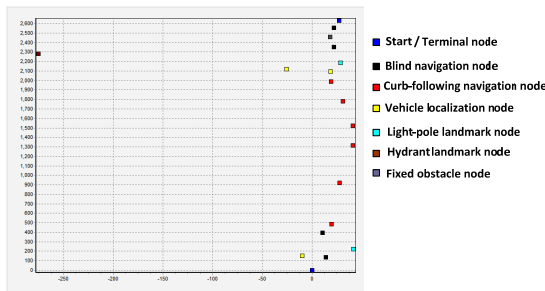
Fig.16: Illustration of a navigation map.

7. CONCLUSIONS

A vision-based autonomous vehicle navigation system for use as a machine guide dog in sidewalk environments has been proposed in this study. To implement such as a system, several new techniques has been proposed, including: 1) a method to train the vehicle system for the purpose of learning guidance parameters related to the environment; 2) a learning process to guide the vehicle to navigate on a sidewalk and construct a navigation map; 3) a new space line detection technique based on the pano-mapping technique; 4) several landmark detection and localization techniques (including those for the curb line,

hydrant, and light pole); 5) techniques for dynamic camera exposure and threshold adjustments which can be employed to handle different lighting conditions; and 6) a new obstacle detection technique using a ground matching table. Good experimental results show the feasibility of the proposed system and methods.
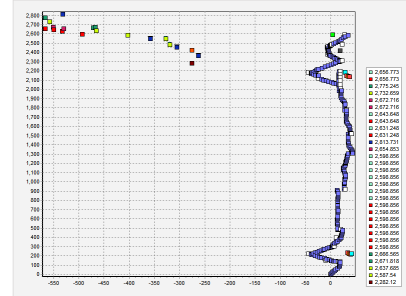
Fig.17: Recorded map of a navigation process (blue points represent vehicle path and other points with different colors represent different localized landmark positions).

REFERENCES

[1] S. E. Yu and D. Kim, "Distance estimation method with snapshot landmark images in the robotic homing navigation," *Proc.s IEEE/RSJ Int'l Conf. on Intelligent Robots & Systems*, pp. 275–280, Taipei, Taiwan, Oct. 2010.

[2] T. Tasaki, S. Tokura, T. Sonoura, F. Ozaki ,and N. Matsuhira, "Mobile robot self-localization based on tracked scale and rotation invariant feature points by using an omnidirectional camera", *Proc. IEEE/RSJ Int'l Conf. on Intelligent Robots & Systems*, pp. 5202-5207, Taipei, Taiwan, Oct. 2010.

[3] C. J. Wu and W. H. Tsai, "Location estimation for indoor autonomous vehicle navigation by omni-directional vision using circular landmarks on ceilings," *Robotics & Autonomous Systems*, vol. 57, No. 5, pp. 546-555, 2009.

[4] B. Siemiątkowska and R. Chojecki, "Mobile robot localization based on omnicamera," *Proc. 5th IFAC/EURON Symp. on Intelligent Autonomous Vehicles (IAV2004)*, Lisbon, Portugal, July 2004.

[5] J. Courbon, Y. Mezouar, and P. Martinet, "Autonomous navigation of vehicles from a visual memory using a generic camera model," *IEEE Trans. on Intelligent Transport. Syst.*, vol. 10, no 3, pp. 392-402, Sept. 2009.

[6] S. Kumar, "Binocular stereo vision based obstacle avoidance algorithm for autonomous Mobile Robots," *Proc. IEEE Int'l Advance Computing Conf.*, pp. 254-259, Patiala, India, March 2009.

[7] Q. Mühlbauer, S. Sosnowski, T. Xu, T. Zhang, K. Kühnlenz, and M. Buss, "Navigation through urban environments by visual perception and interaction," *Proc. IEEE Int'l Conf. on Robotics & Automation*, pp. 1907–1913, Kobe, Japan, 2009.

[8] S. W. Jeng and W. H. Tsai, "Using pano-mapping tables to unwrapping of omni-images into panoramic and perspective-view Images," *Proceeding of IET Image Processing*, vol. 1, no. 2, pp. 149-155, June 2007.

[9] C. J. Wu and W. H. Tsai, "An omni-vision based localization method for automatic helicopter landing assistance on standard helipads," *Proc. 2nd Int'l Conf. on Computer & Automation Engineering*, vol. 3, pp. 327–332, Singapore, 2010.